Topics in Catalysis (2023) 66:922–932
https://doi.org/10.1007/s11244-022-01726-y

ORIGINAL PAPER

Manganese Based Perovskites in Soot Oxidation: Far from Noble Metals?

Elena Brusamarello[1] · Giacomo Peron[1] · Filippo Nigrelli[1] · Antonella Glisenti[1,2]

Accepted: 10 October 2022 / Published online: 2 November 2022

Abstract
Mn-based catalysts for soot oxidation have been developed without noble metals. The compositions are $LaMn_{0.9}Co_{0.1}O_3$, $La_{0.9}K_{0.1}Mn_{0.9}Co_{0.1}O_3$ (LKMC), $Sr_{0.9}K_{0.1}Mn_{0.9}Co_{0.1}O_3$ and 0.1 K/$La_{0.9}Mn_{0.9}Co_{0.1}O_3$: Mn provides stability to the structure both in oxidizing and reducing atmospheres and efficiently exchanges oxygen. Moreover, Co doping enhances soot oxidation. Adding La or Sr as A-site cation in the perovskite composition allows comparing the behaviors of the so-obtained perovskites, and K doping was chosen to increase catalytic activity both in soot and NO_x removal. After the wet synthesis, the catalysts were tested for soot oxidation in presence of oxygen and nitrogen monoxide in overstoichiometric oxygen content. Temperature Programmed Oxidation tests were performed and double doping increases the oxidative catalytic activity: LKMC shows the lowest soot conversion temperature (306 °C, soot in tight contact with the catalyst). Sr doping results in worse performances, due to the formation of $SrCO_3$. K incorporation helps oxygen vacancies formation, beneficial to the catalytic activity, through the Mars-van Krevelen mechanism.

Keywords Perovskite · TWC · Soot oxidation · Catalysis · Environment · Manganese

1 Introduction

Soot is dangerous for human health and climate change [1]. To prevent soot emission different and complementary approaches are possible: the design of reactors or engines may be optimized, highly efficient filters can be applied and/or catalysts can be used to lower the ignition temperature of soot, with regards to soot elimination by oxidation.

Commercially the current, and one of the first, solution employed for Diesel engines in automotive sector is the use of the so-called Diesel Particulate Filters (DPFs). They are fabricated in a similar way as Three Way Catalytic converters (TWC): they comprise a monolith (traditionally made of cordierite, or silicon carbide for higher mechanical resistance at high temperature) with a honeycomb structure with high surface areas. Through the mechanism called surface filtration or coke filtration, soot is deposited on the surface of the device and periodically combusted. Technologic progress in this field brought also the use of the so-called Continuous Regeneration Trap (CRT), patented by Johnson Matthey. This device combines a DPF filter with a Pt-based pre-oxidizer which converts CO, hydrocarbons and NOx to CO_2, H_2O and NO_2. NO_2 is then used to oxidize soot to carbon dioxide. Later on a Four Way Catalyst was developed, again in the attempt of combining in a single device the TWC features with soot oxidation activity. The main drawback of such devices is still the massive use of noble metals in the active phase (e.g., Pt, Pd and Rh), and the present work is an endeavor to investigate the possibility of using non-noble metal based perovskites, already known for their TWC activity, in soot oxidation reactions. Other examples of this strategy are to be found in literature [2].

The use of noble metal free catalysts could allow to obtain low cost and sustainable soot abatement devices. Perovskites type oxides are promising catalysts [3] because of their capacity of achieving the simultaneous removal of NO_x and diesel soot in the presence of oxygen [4–7]. Among the perovskites, $LaMnO_3$-based ones are characterized by the higher efficiency. To improve the catalyst performances alkali and alkali-metals are exploited [8–11]: Including potassium in the structure seems to help in this

✉ Elena Brusamarello
elena.brusamarello@phd.unipd.it

[1] Department of Chemical Sciences, University of Padova, Via F. Marzolo, 1, 35131 Padua, Italy

[2] CNR-ICMATE, INSTM, Via F. Marzolo, 1, 35131 Padua, Italy

senso [7, 12].The mechanisms through which superior performances are obtained are not yet fully understood but a relevant role seems to be played by electron exchange, soot morphology modification and finally decreased stability of surface carbonates [13]. The contribution of all these phenomena can differ for the specific type of oxidic catalysts. In the present contribution we focused on cobalt-doped manganese-based perovskites. In particular, the effect of K on $LaMn_{0.9}Co_{0.1}O_3$ and $SrMn_{0.9}Co_{0.1}O_3$ is studied; moreover, the insertion of K into the crystalline cell and, on the other side, the deposition on the surface have been compared in terms of catalytic efficiency.

Mul et al. [14] identified two different procedures to test soot oxidation in presence of a catalyst: loose and tight contact. Loose contact represents a situation closer to the real one, as catalyst and soot are simply mixed together with a spatula; tight mode prescribes instead a much more intimate contact between the two species, obtained by crushing them in a mortar.

2 Materials and Methods

2.1 Synthesis

The samples were prepared by citrate method [15] starting from La_2O_3 (Sigma-Aldrich, pure), $Sr(NO_3)_2$ (Aldrich ≥ 98%), Manganese(II) acetate tetra hydrate (Sigma-Aldrich ≥ 99%), K_2CO_3 (Aldrich 95%) and $Co(NO_3)_2{\cdot}6H_2O$ (Sigma-Aldrich 98%). Carbonate and nitrate precursors were dissolved in an aqueous solution while lanthanum solution was obtained by mineralizing the corresponding oxide with nitric acid. A solution of monohydrate citric acid (Sigma Aldrich ≥ 99.0%) was added: its molar ratio was 1.9:1 with respect to the total amount of cations. Then solution is then heated up to 80 °C in air to promote water evaporation and to obtain a pink wet-gel. The gel is slowly heated up to 400 °C for 2 h in air to decompose the organic framework and the obtained powder samples were ground and calcined at 700 °C ($LaMn_{0.9}Co_{0.1}O_3$—LMC, $La_{0.9}K_{0.1}Mn_{0.9}Co_{0.1}O_3$—LKMC) and 800 °C ($Sr_{0.9}K_{0.1}Mn_{0.9}Co_{0.1}O_3$—SKMC) for 6 h to obtain the perovskite. The nanocomposite, $KO_x/LaMn_{0.9}Co_{0.1}O_3$—K/LMC, was obtained by wet impregnation of the LMC perovskite powder with a solution of K^+ obtained by dissolving the carbonate in order to reach the same atomic composition of the LKMN catalyst. The suspension was stirred 24 h and then the solvent was slowly removed by heating at 90 °C. The final heat treatment was carried out at 500 °C for 3 h (the desorption of K was observed at temperatures higher than 600 °C).

2.2 Characterization

The XPS measurements were carried out with a Perkin Elmer Φ 5600ci Multi Technique System. The spectrometer was calibrated by assuming the binding energy (BE) of the Au $4f_{7/2}$ line to be 84.0 eV with respect to the Fermi level. Both extended spectra (survey—187.85 eV pass energy, 0.8 eV $step^{-1}$, 0.05 s $step^{-1}$) and detailed spectra (for Mn 2p, Co 2p, La 3d, Sr 2p, K 1s, O 1s and C 1s–23.50 eV pass energy, 0.1 eV $step^{-1}$, 0.1 s $step^{-1}$) were collected with a standard Al Kα source working at 200 W. The standard deviation in the BE values of the XPS line is 0.10 eV. The atomic percentage, after a Shirley-type background subtraction [16], was evaluated by using the PHI sensitivity factors [17]. The peak positions were corrected for the charging effects by considering the C 1s peak at 285.0 eV and evaluating the BE differences [18].

The XRD analyses were performed with a Bruker D8 Advance diffractometer with Bragg–Brentano geometry using a Cu Kα radiation (40 kV, 40 mA, $\lambda = 0.154$ nm). The data were collected at 0.03°, with a counting time of 7s/step in the (2θ) range from 20° to 70°. The crystalline phases were identified by the search-match method using the ICDD (International Centre for Diffraction Data) database. Temperature Programmed Reduction (TPR), and specific surface area (BET, Brunauer–Emmett–Teller) measurements were performed with an Autochem II 2920 Micromeritics, equipped with a TCD detector. The H_2-TPR measurements were carried out in a quartz reactor by using 50 mg of sample and heating from RT to 900 °C at 10 °C min^{-1} under a constant flow of H_2 5% in Ar (50 ml min^{-1}). TPR samples were previously outgassed with He (50 ml min^{-1}) at RT. In BET measurements 100 mg of sample were used; before measurement the sample was treated at 350 °C for 2 h under a constant flow of He (50 ml min^{-1}); each surface area value obtained was the average of three consecutive measurements [19].

Field emission-scanning electron microscopy and EDX measures were carried on a Zeiss SUPRA 40VP. Morphological analysis and EDX analysis were carried out setting the acceleration voltages at 20 kV.

2.3 Catalytic Activity Tests

The catalytic tests are carried out in a quartz reactor (6 mm ID) with a packed bed of powders; the temperature was monitored by a thermocouple right upstream of the bed. The inert carrier was always Ar. The flow rates were controlled by thermal mass flow meters (Vögtlin). The composition of the gas mixture (before and after reaction) was

measured by Gas Chromatography (Agilent 7890A), with a TCD detector and 13X (60/80 mesh, 1.8 m) and Porapak Q (1.8 m) columns. Temperature ramp involved a fast heating (10 °C min^{-1}) until 150 °C, which should favor CO_2 desorption from the sample, and a slow ramp (1 °C min^{-1}) until 450 °C. Injection of the products at the GC was carried out every eight minutes from a continuous stream, allowing us to detect also the possible production of CO in competition to CO_2 from the combustion, an occurrence that, however, was never detected. Soot was added in 1:10 ratio in tight contact mode. If an oxygen-transfer step is involved, then the contact between catalyst and soot and, experimentally, the method used to bring them in contact, is crucial to the catalytic activity. Standard Printex-U carbon black is used to simulate soot. To enhance the catalyst answer and emphasize the difference in the behaviors, tight contact was preferred over loose one. This allows a better evaluation of the effect of the different A-site cation (K vs Sr) and of their insertion into the perovskite cell with respect to the surface deposition.

The OSC test was carried out in the same setup, employing 50 mg of catalyst, and composed of two steps. In the first one, the catalyst was subjected to 1 h of oxidation treatment in synthetic air (80% N_2/20% O_2) at the fixed temperature of 300 °C. The second step, spaced with 2 min He flow, was a CO-TPR reaction at the same fixed temperature, using a 5%CO/He atmosphere. Gas flow was always kept at 100 ml min^{-1}.

Table 1 Composition of the studied catalyst and specific surface area (m^2g^{-1})

Sample	Acronym	BET specific surface area (m^2g^{-1})
$LaMn_{0.9}Co_{0.1}O_3$	LMC	25
$La_{0.9}K_{0.1}Mn_{0.9}Co_{0.1}O_3$	LKMC	21
$K10\%/LaMn_{0.9}Co_{0.1}O_3$	K/LMC	20
$Sr_{0.9}K_{0.1}Mn_{0.9}Co_{0.1}O_3$	SKMC	6

3 Results and Discussion

3.1 Chemical and Structural Characterization

The materials prepared are listed in Tables 1and 2, together with the results of XRD and H_2-TPR analysis. All diffraction peaks of the La-containing perovskites can be assigned to the rhombohedral geometry. (JCPDS 72-1156 (C)), (Fig. 1) while the hexagonal one is observed in SKMC. Doping with K(I) causes the shift of the whole XRD pattern toward lower angles (because of the difference in ionic radii K(I) = 1.38 Å, La(III) = 1.061 Å) [20] confirming the penetration of K into the perovskite cell. No secondary phases are observed.

BET surface area values are summarized in Tables 1 and 2. The values obtained in the catalysts containing K are only slightly lower than that of LMC. The specific surface area of SKMC is, in contrast, significantly lower; this result is probably a consequence of the higher calcination temperature (800 instead of 700 °C) necessary to obtain the perovskite phase.

The XP spectra are compared in Fig. 2. The Mn 2p XP peaks are centered at 642.2–642.5 and 653.6–654.0 eV for the 3/2 and 1/2 components, respectively, a position which is typical of Mn in oxides; it is difficult, however, to distinguish between Mn(III) and Mn(IV) [21]. Cobalt is rather absent in surface, in contrast, and is slightly more relevant in the region below; this suggests that eventual electronic interaction with Mn cannot be really significant. No significant differences are observed when K is also present or when Sr substitutes La. La 3d peak position (834.2–834.6 and 851.0–851.4 eV, for $3d_{5/2}$ and $3d_{3/2}$, respectively) and shape (shake-up contributions at 840 and 858 eV) are

Table 2 Composition of the studied catalyst, crystalline structure and H_2 up-take data obtained by means of H_2-TPR

Sample	Crystalline structure		Total H_2 up-take (mol H_2mol^{-1})	Mn(III)/Mn(II) Co(II)/Co(0) (%)	Mn(IV)/Mn(III) Co(III)/Co(II) (%)
$LaMn_{0.9}Co_{0.1}O_3$	Rhombohedral	Theoretical	0.60	8	92
		Experimental	0.59	41	59
$La_{0.9}K_{0.1}Mn_{0.9}Co_{0.1}O_3$	Rhombohedral	Theoretical	0.65	23	77
		Experimental	0.54	46	54
$K10\%/LaMn_{0.9}Co_{0.1}O_3$	Rhombohedral	Theoretical	0.60	8	92
		Experimental	0.40	43	57
$Sr_{0.9}K_{0.1}Mn_{0.9}Co_{0.1}O_3$	Hexagonal	Theoretical	1.05	48	52
		Experimental	0.97	81	19

The up-take data are expressed as mol H_2mol^{-1} sample; the attribution to the reduction phenomena (determined by fitting the experimental curves) are compared with the theoretical ones determined considering that all K is inserted into the crystalline cell and determined the formation of Mn(IV). The data in the last two columns are percentages expressing the relative amount of hydrogen consumed for each reduction process

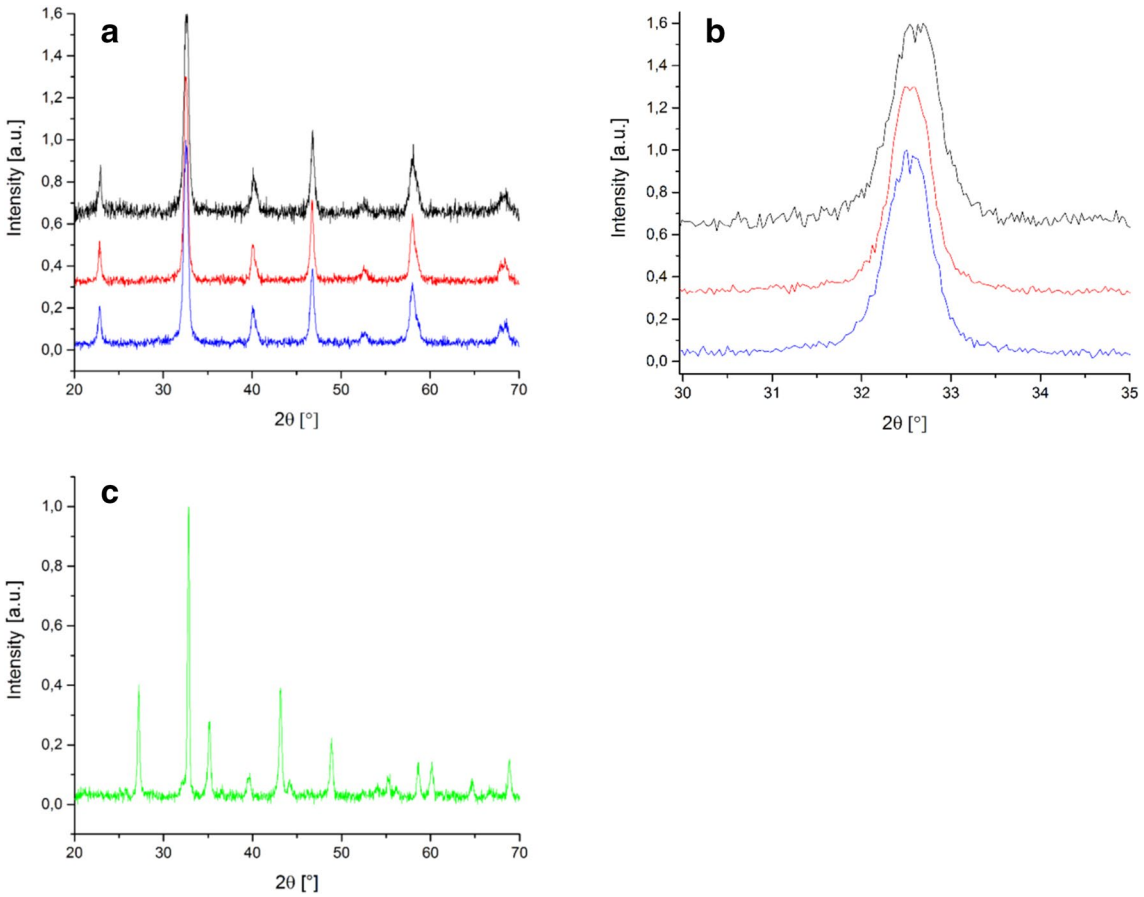

Fig. 1 XRD patterns of: **a** $LaMn_{0.9}Co_{0.1}O_3$ (blue), $La_{0.9}K_{0.1}Mn_{0.9}Co_{0.1}O_3$ (red), 0.1 $K/LaMn_{0.9}Co_{0.1}O_3$ (black), **b** Detail 30–35°; **c** $Sr_{0.9}K_{0.1}Mn_{0.9}Co_{0.1}O_3$ (green)

consistent with how expected for La(III) in perovskites and are not modified by doping or by the deposition of K. Sr 3d peak shows two doublets whose 5/2 positions, at 132.8 and 133.6 eV, respectively, suggest the presence, beside the perovskite, of carbonate species, compatible with C1s spectra.

Two main signals compose the O 1 s spectra, as obtained deconvoluting the spectra: the peak at 529.5–530.0 eV is due to the perovskite lattice oxygen whereas the one at about 532.0 eV at oxygen in hydroxides and carbonates; this last contribution is more evident in SKMC [18, 21–26]. The deconvolution procedure for O1s peaks is reported in the Supplementary Information file.

In all catalysts, XPS quantitative analysis (Table 3) reveals the surface segregation of oxygen, consistent with the formation of hydroxyl and carbonate groups, as denoted by qualitative analysis. In LMC surface segregation of Mn is evident, and it is not significantly affected by the insertion of K. Also K shows an attitude to surface segregation. The propensity of K toward surface segregation is particularly evident when Sr substitutes La. It is noteworthy that, in K/LMC, K is less present in surface than expected, consistently with its frequently reported desorption trend [27, 28]. The "after reaction" compositional values are discussed below, in the section "Reactivity".

SEM images are grouped in Fig. 3. Qualitatively it can be appreciated the higher dimension of SKMC particles compared with samples from the same group, identified to reach about 100 nm. It is not clearly distinguishable the presence of K_2O in K/LMC from the simple visual analysis, but the surface presents a higher variability and irregularity that can be a trace for the presence of different phases unhomogeneously distributed.

The H_2-TPR curves of the different catalysts are compared in Fig. 4. In all cases the presence of two groups of signals centered around 300–400 °C (Mn(IV) to Mn(III)) and 600–800 °C (Mn(III) to Mn(II)) is evident. The reduction of cobalt is expected to contribute in a low amount to both the groups of signals (Co(III) to Co(II) around 440 °C and Co(II) to Co(0) around 500–600 °C). [29]

Focusing on the lower temperature signals two main contributions are observed in LMC at 320 and 388 °C, whereas at higher temperature a broad signal is observed around

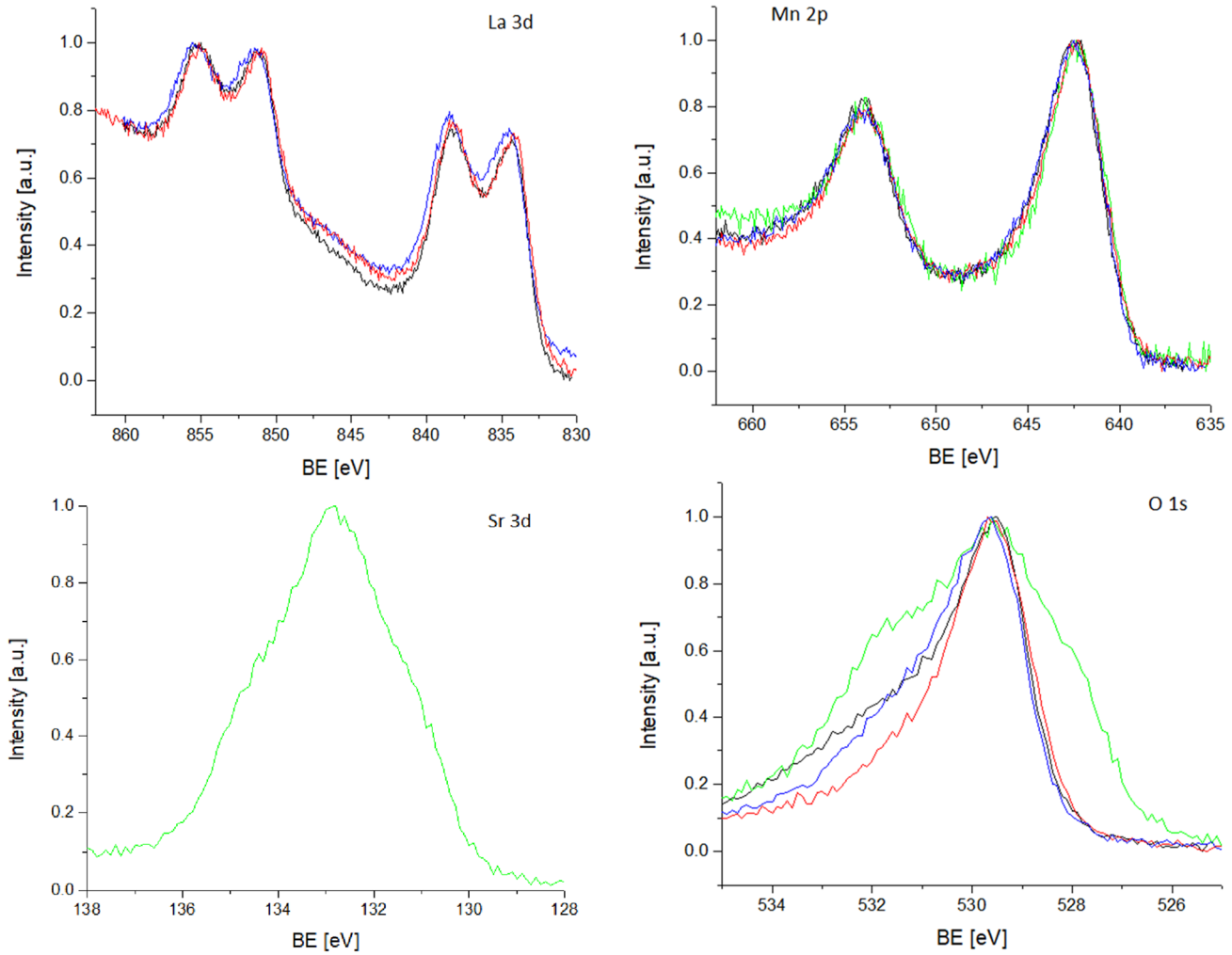

Fig. 2 XP spectra obtained for $LaMn_{0.9}Co_{0.1}O_3$ (blue), $La_{0.9}K_{0.1}Mn_{0.9}Co_{0.1}O_3$ (red), 0.1 K/$LaMn_{0.9}Co_{0.1}O_3$ (black), $Sr_{0.9}K_{0.1}Mn_{0.9}Co_{0.1}O_3$ (green)

800 °C. The Gaussian fitting procedure on the TPR peaks reveals, in the low temperature signals group, minor contributions around 157, 218, and 270 °C. The comparison with literature data suggests to attribute these last signals to the reduction of surface oxygen species [30]. Calculating the expected moles of hydrogen consumed during the Temperature- Programmed Reaction (considering the stoichiometry of the perovskite) it was possible to estimate the percentage of each species reacting the in analyzed sample. Oxygen species contribute less than 10% to the total H_2-consumption. The signals at 321 and 388 °C, consistent with the reduction of Mn(IV), contributes for about 30% of hydrogen consumption. The remaining consumption is observed around 800 °C and corresponds to the reduction of Mn(III) [31, 32]. The H_2-uptake corresponds to 0.24 mol H_2mol^{-1} LMC at low temperature and 0.35 mol H_2mol^{-1} LMC at higher temperature. According to literature, the hydrogen consumption below 500 °C was attributed to the reduction Mn(IV) to Mn(III) of some Mn(IV) present in the perovskite structure, however, based on the hydrogen consumption values, it is likely that the reduction process of Mn(III) to Mn(II) partially occurred in that temperature range. The effect of Co on enhancing the reducibility of Mn(III) cannot be excluded but this hypothesis is not supported by XPS data. The reducibility of Mn(III) at lower temperature was observed to depend on the amount of complexing agent (citric acid) and on the textural properties of the catalyst [33]. In particular, the Mn(III) reduction seems to be favored by higher specific surface area and lower size of the particles. The H_2 uptake between 150 and 400 °C (which can give a rough idea of the reducibility) is 0.24 mol H_2mol^{-1} (Mn + Co) which corresponds to 40% of the Mn + Co ions in 1 mol of perovskite.

The insertion of K into the perovskite cell determines a slight increment of the surface oxygen species which contribute to the total consumption for 12.5%. The H_2-uptake at higher temperature decreases from 0.35 to 0.29 mol H_2mol^{-1} perovskite. Also the total uptake decreases from 0.59 to 0.54 mol H_2mol^{-1} (Mn + Co). The H_2 uptake at

Table 3 XPS and EDX quantitative analysis of the catalysts; the nominal compositions obtained from the weighted amounts are reported for comparison

		La	K	Mn	Co	O	K/La	Mn/La	(Co+Mn)/(K+La))
LMC	XPS	15.7(42.2)	–	21.0(56.5)	0.5(1.3)	62.9	–	1.3	1.4
	EDX	18.1(47.9)	–	16.7(44.2)	3.0(7.9)	62.2	–	0.9	1.1
Nominal	As prepared	20.0(50.0)	–	18.0(45.0)	2.0(5.0)	60.0	–	0.9	1.0
	XPS After reaction	12.6(45.2)	–	11.9(42.6)	3.4(12.2)	72.1	–	0.9	1.2
LKMC	XPS	11.6(28.3)	5.8(14.2)	23.1(56.3)	0.5(1.2)	59.0	0.5	2.0	1.4
	EDX	16.0(42.1)	1.9(5.0)	18.1(47.6)	2.0(5.4)	62.0	0.1	1.1	1.1
Nominal	As prepared	18.0(45.0)	2.0(5.0)	18.0(45.0)	2.0(5.0)	60.0	0.1	1.0	1.0
	XPS After reaction	2.2(4.9)	26.0(57.5)	7.2(15.9)	9.8(21.7)	54.8	11.8	3.3	0.6
K/LMC	XPS	12.4(37.1)	2.5(7.6)	18.2(54.6)	0.3(0.7)	66.6	0.2	1.5	1.2
	EDX	14.7(45.1)	1.1(3.4)	14.9(45.7)	1.9(5.8)	67.3	0.1	1.0	1.1
Nominal	As prepared	18.0(45.0)	2.0(5.0)	18.0(45.0)	2.0(5.0)	60.0	0.1	1.0	1.0
	XPS After reaction	3.1(5.4)	32.6(57.1)	8.5(14.9)	12.9(22.6)	42.9	10.5	2.7	0.6
		Sr	K	Mn	Co	O	K/Sr	Mn/Sr	(Co+Mn)/(K+Sr)
SKMC	XPS	15.1(39.3)	8.1(20.9)	13.7(35.6)	1.7(4.3)	61.4	0.5	0.9	0.7
	EDX	13.7(50.4)	0.8(3.0)	11.4(42.0)	1.3(4.6)	72.9	0.1	0.8	0.9
Nominal	As prepared	18.0(45.0)	2.0(5.0)	18.0(45.0)	2.0(5.0)	60.0	0.1	1.0	1.0
	XPS After reaction	13.1(23.7)	29.3(52.9)	9.5(17.1)	3.5(6.3)	44.6	2.2	0.7	0.3

Values in brackets indicate the percentage without considering oxygen contributions (cation-only composition). “After reaction” values are taken post soot oxidation test by XPS

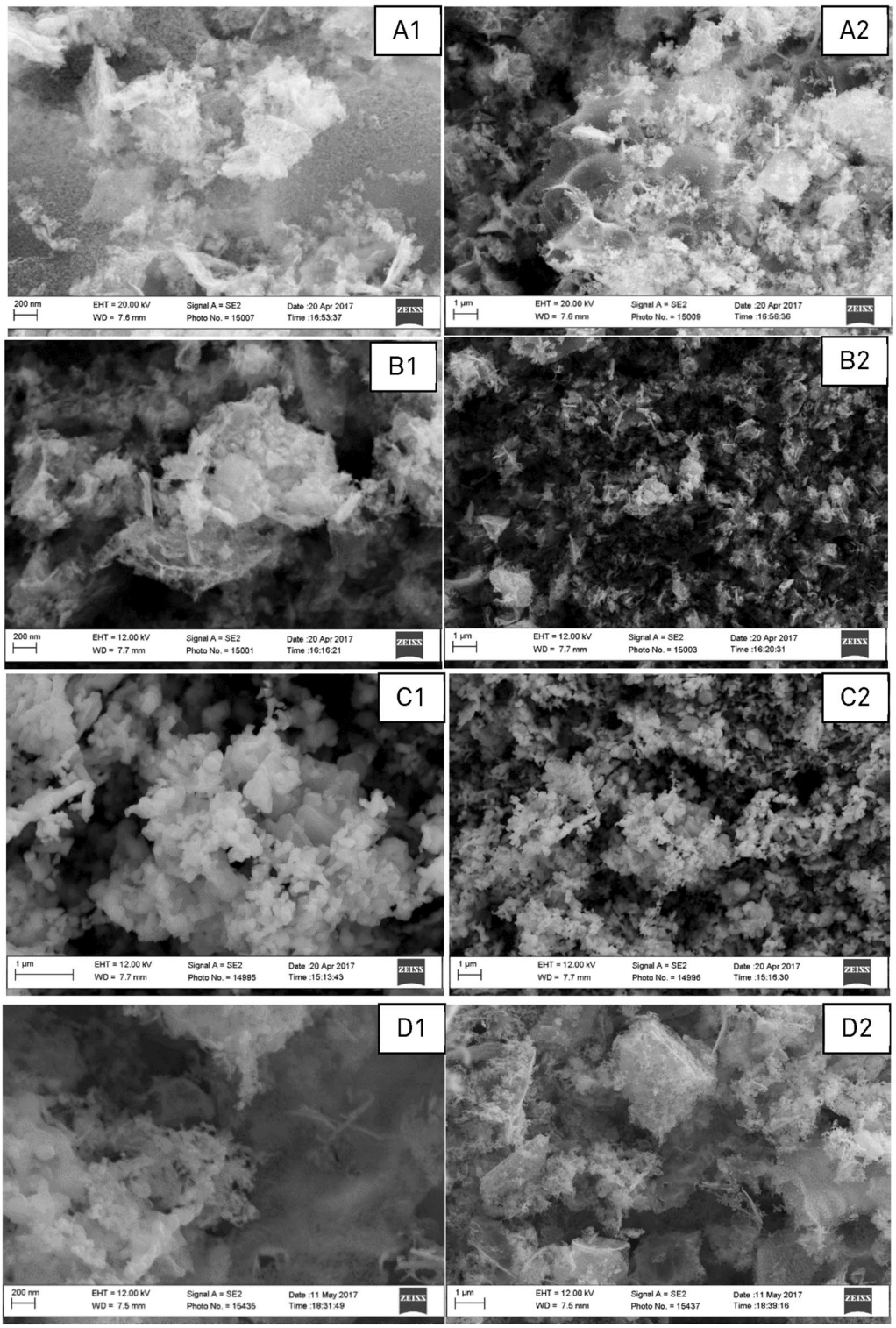

Fig. 3 SEM images: **A** K/LMC; **B** LMC; **C** SKMC; **D** LKMC. Images labelled with "1" are taken at 105 K magnification, images labelled with "2" at 104 K magnification

lower temperature is 37% of the expected. The reducibility decreases even more when K is deposited on the surface of LMC (28%). The insertion of Sr inside the perovskite cell in substitution of La is expected to favor the formation of Mn(IV) and thus the reducibility. Consistently the H_2-uptake at low temperature is 0.78 mol $H_2 mol^{-1}$ (Mn + Co) and the reducibility is 74%. Noteworthy in the K/LMC and SKMC catalysts no traces of surface oxygen species (reduced at

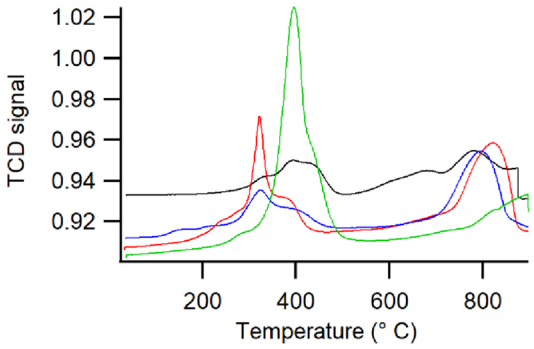

Fig. 4 TPR curves obtained for $LaMn_{0.9}Co_{0.1}O_3$ (blue), $La_{0.9}K_{0.1}Mn_{0.9}Co_{0.1}O_3$ (red), 0.1 $K/LaMn_{0.9}Co_{0.1}O_3$ (black), $Sr_{0.9}K_{0.1}Mn_{0.9}Co_{0.1}O_3$ (green)

Table 4 Theoretical average Mn oxidation state obtained by H_2-TPR

Sample	Mn oxidation state (average)
LMC	3
LKMC	3.2
SKMC	4.1
K/LMC	3

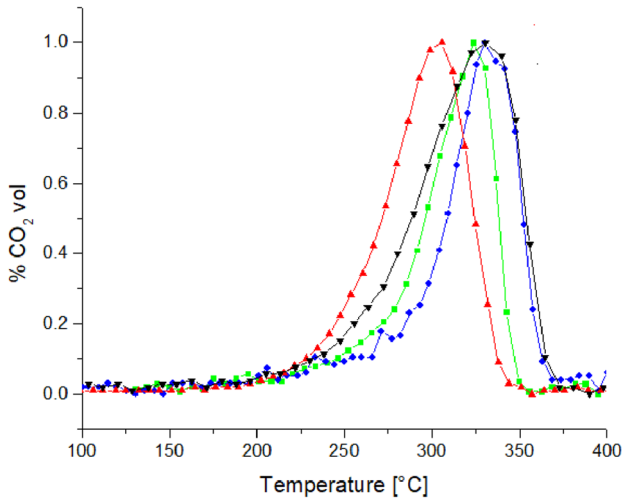

Fig. 5 CO_2 formed from soot oxidation, as a function of temperature, for the different catalysts: $LaMn_{0.9}Co_{0.1}O_3$ (blue), $La_{0.9}K_{0.1}Mn_{0.9}Co_{0.1}O_3$ (red), 0.1 $K/LaMn_{0.9}Co_{0.1}O_3$ (black), $Sr_{0.9}K_{0.1}Mn_{0.9}Co_{0.1}O_3$ (green)

temperature lower than 300 °C) is observed. A summary of the results of the H_2-TPR is reported in Tables 1 and 2, and the relative amount of consumed hydrogen for each reduction process is included.

A theoretical average oxidation state for Mn could be also calculated with the H_2-TPR data, taking into account the charge balance in the perovskite formula. The so-obtained values are reported in the following Table 4. Consistently with how expected the oxidation state is higher and near to 4 when A-cation is Sr and 3 when A is La.

3.2 Catalytic Activity

The catalytic behavior in the soot oxidation is compared in Fig. 5. The temperature of maximum conversion of soot and the CO_2 production curve shape underline that the insertion K into the perovskite cell improves the performance of the catalysts toward soot oxidation. The worst results are obtained with the un-activated LMC. In all cases, however, the presence of a catalyst favors the soot oxidation; as demonstrated by blank tests in literature [34].

The soot oxidation in absence of catalyst is suggested to proceed through the following steps: firstly, molecular oxygen is chemisorbed onto the soot surface; the dissociative chemisorption allows oxygen atoms to interact with the surface carbon atoms and form a complex solid [35]. At the end the solid complex desorbs subtracting a carbon atom from the soot particle [36].

The adsorption of the oxidant on the surface active site of carbon and the desorption of the products strongly depend on the oxidant concentration, on the amount of active sites, on the coverage degree and sticking fault. It is reasonable to consider the dissociative chemisorption of oxygen as the rate determinant step. The reactivity of NO_2 is higher with respect to that of O_2; it is suggested that NO_2 can form surface complex molecules of the type C–NO_2 and C–ONO capable of decomposing with increasing temperature forming CO, CO_2 and NO [36].

In presence of oxide-based catalysts the reaction mechanism is more complicated and involves the interaction of perovskite and soot particles. It is suggested that several steps follow: adsorption of oxygen on the catalyst, exchange of activated oxygen species (such as O^- and O^{2-}) from catalyst to the carbon surface, formation of surface oxygen containing (SOC) complex molecules, desorption of SOCs. The catalytic activity is, in this case, affected by the capability of the catalyst to promote the formation and exchange of SOCs [37].

Li et al. suggest four reaction mechanisms that simultaneously occur during soot combustion: soot oxidation in the soot/catalyst interface carried out by the active species O^{2-} and O^- formed by interaction of oxygen with the surface oxygen vacancies; catalytic oxidation of NO to NO_2 on the catalyst surface; N-containing species adsorb on the catalyst surface and can migrate toward the soot particles; NO oxidation to nitrates and nitrites that can oxidize soot giving rise to CO_2 and N_2; adsorption of NO_2 on the soot surface and direct reaction (of NO_2 or NOx resulting from decomposition) with surface carbon [38].

All catalysts are active in the soot oxidation: the temperature of maximum combustion, considered as a value to compare the catalytic activity, T_m, decreases of, at least, 60 °C with respect of the case without catalyst. The more active catalyst, however, is LKMC with a T_m of 306 °C whereas the worst is LMC. The substitution of La with Sr moves toward lower values (around 250 °C) the temperature at which the catalysts start its activity but the T_m is similar to that of LMC (323 vs 330 °C). It is interesting to observe that when K is deposited on the LMC surface the catalyst seems to activate at a temperature similar to that of the LKMC but the T_m is almost coincident to that of LMC).

LKMC is the catalyst characterized by the higher surface segregation of the B-Cations; moreover, the TPR reveals the higher relative amounts of species reduced at lower temperatures (280–320 °C) so suggesting the contribution of surface oxygen active species to switch the reaction and of Mn(IV) species. Mn(IV) is present in higher amount in the SKMC catalysts but the reduction temperature is shifted at higher temperature (around 400 °C). In this last case the almost complete absence of oxygen surface active species is underlined by a Gaussian fitting procedure of H_2-TPR peaks.

The XPS analysis carried out on the catalysts after reaction reveals a significant surface segregation of Co in LMC; in the other catalysts the surface segregation of K is present. The surface segregation of cobalt in SKMC is less marked while no particular difference is observed between LKMC and K/LMC. A possible explanation of the phenomenon of Co segregation after reaction is that Co, being more prone to reduction, is drawn to the surface by the reducing surface potential imposed by contact with the soot.

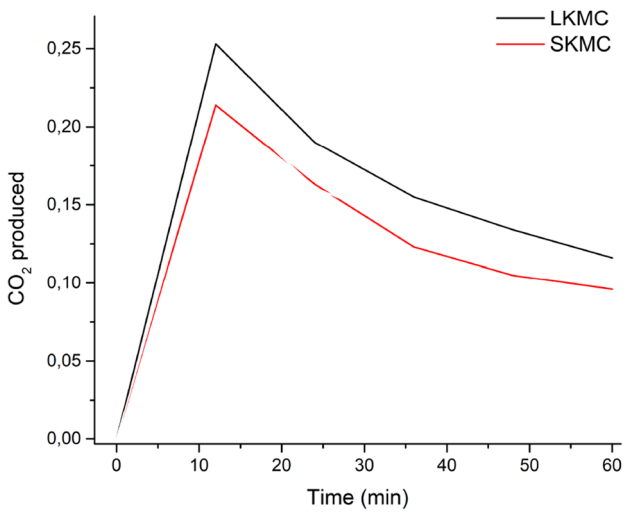

Fig. 6 CO_2 formed from CO oxidation after 1 h of oxidation treatment at 300 °C as a function of time: LKMC (black) and SKMC (red)

Figure 6 shows the carbon dioxide profiles obtained on the K-doped catalysts tested for their Oxygen Storage Capacity (OSC).

Hydrogen-TPR had denoted a faster reduction kinetic when K was present in the structure. In this particular test, the first maximum, sampled at 12 min from the beginning of the test, is related to the most reactive oxygen, and the degree of convergence towards 0 yield can instead give insights on the transport and active replenish of the surface oxygen species. We already argued that K insertion mainly affects surface reactivity, increasing oxygen retention on the surface, whereas Sr employment can help in stabilizing the structure and increase oxygen supply to the reaction sites.

LKMC significantly outperforms SKMC, suggesting that with combined K-doping, helping chemisorption of oxidant species, and Co, that has already proven to induce higher oxygen mobility and structural modifications, the mechanism of the reaction can find a good balance between the two paths of activated oxygen species creation. Indeed surface chemisorption of oxygen and transport of oxygen from the bulk to the surface are the two driving forces of the reaction of soot oxidation in this process. Oxygen transport contribution, intimately related to ion mobility within the structure, becomes more important when doping with Sr. Cobalt was found by Royer et al. to present a good redox activity even at low temperatures, favoring ion mobility in the bulk [39]. Finally, SKMC benefits from the presence of Co, but its transport activity is undermined by K presence.

4 Conclusion

The scope of this manuscript is the investigation and development of innovative perovskite catalysts with the aim of a possible application in the abatement of carbon soot from diesel engines in the automotive sector. The employment of novel materials, such as the ones suggested from the present work, with a reduced content of noble metals is a challenging yet urgent task in this technologic branch. Therefore, the materials here proposed have been tested for soot oxidation in presence of oxygen and NO, with an excess of oxygen to emulate the conditions of a real diesel engine exhaust mixture, and for their oxygen storage capacity, to get a deeper insight on their mechanistic aspects.

The compositions chosen arise from redox considerations: Mn, stable both in reducing and oxidizing environments, is a good oxygen donating element in perovskite oxides. In the B-site, furthermore, Co is known for soot and NO oxidation. In the A-site the K-doping resulted in an increased catalytic activity both for soot oxidation and

NO_x conversion. K deposition was also investigated to shed light on its significance when outside the structure.

Temperature Programmed Oxidation test (i.e., catalytic activity assessment) in presence of NO, oxygen and soot showed that the double doping (Co and K) increases notably the catalytic activity of the material in the oxidation reaction: LKMC is able to fully oxidize soot at 306 °C, a considerably lower temperature than without any catalyst. Sr-doped samples are still quite active, but less than the counterpart without Sr. Another interesting result is the different behavior for the K-doped sample and the K-deposited one: it is likely that K-doping only is able to promote oxygen vacancies formation.

Considering all these aspects, both from compositional points of view and from catalytic and OSC tests, LKMC seems to be a good trade-off between surface activity guaranteed by K and the importance of oxygen from the lattice thanks to the presence of Co.

Supplementary Information The online version contains supplementary material available at https://doi.org/10.1007/s11244-022-01726-y.

Funding Open access funding provided by Università degli Studi di Padova within the CRUI-CARE Agreement.

Declarations

Conflict of interest The authors have no competing interests to declare that are relevant to the content of this article.

References

1. Jacobson MZ (2010) Short-term effects of controlling fossil-fuel soot, biofuel soot and gases, and methane on climate, arctic ice, and air pollution health. J Geophys Res Atmos 115(14):14209. https://doi.org/10.1029/2009JD013795
2. Mishra A, Prasad R (2014) Preparation and application of perovskite catalysts for diesel soot emissions control: an overview. Catal Rev 56(1):57–81. https://doi.org/10.1080/01614940.2014.866438
3. Hernández-Giménez AM, Castelló DL, Bueno-López A (2014) Diesel soot combustion catalysts: review of active phases. Chem Pap 68(9):1154–1168. https://doi.org/10.2478/s11696-013-0469-7
4. Peng X, Lin H, Shangguan W, Huang Z (2007) A highly efficient and porous catalyst for simultaneous removal of NO_x and diesel soot. Catal Commun 8(2):157–161. https://doi.org/10.1016/j.catcom.2006.04.015
5. Teraoka Y, Nakano K, Shangguan W, Kagawa S (1996) Simultaneous catalytic removal of nitrogen oxides and diesel soot particulate over perovskite-related oxides. Catal Today 27(1–2):107–113. https://doi.org/10.1016/0920-5861(95)00177-8
6. Teraoka Y, Nakano K, Kagawa S, Shangguan WFF (1995) Simultaneous removal of nitrogen oxides and diesel soot particulates catalyzed by perovskite-type oxides. Appl Catal B Environ 5(3):L181–L185. https://doi.org/10.1016/0926-3373(94)00059-X
7. Teraoka Y, Kanada K, Kagawa S (2001) Synthesis of LaKMnO perovskite-type oxides and their catalytic property for simultaneous removal of NO_x and diesel soot particulates. Appl Catal B Environ 34(1):73–78. https://doi.org/10.1016/S0926-3373(01)00202-8
8. Legutko P, Kaspera W, Jakubek T, Stelmachowski P, Kotarba A (2013) Influence of potassium and NO addition on catalytic activity in soot combustion and surface properties of iron and manganese spinels. Top Catal 56(9–10):745–749. https://doi.org/10.1007/s11244-013-0026-1
9. Li Q, Wang X, Xin Y, Zhang Z, Zhang Y, Hao C, Meng M, Zheng LL, Zheng LL (2015) A unified intermediate and mechanism for soot combustion on potassium-supported oxides. Sci Rep 4(1):4725. https://doi.org/10.1038/srep04725
10. Pacultová K, Draštíková V, Chromčáková, Bílková T, Kutláková KM, Kotarba A, Obalová L (2017) On the stability of alkali metal promoters in Co mixed oxides during direct NO catalytic decomposition. Mol Catal 428:33–40. https://doi.org/10.1016/j.molcata.2016.11.038
11. Shang Z, Sun M, Che X, Wang W, Wang L, Cao X, Zhan W, Guo Y, Guo Y, Lu G (2017) The existing states of potassium species in K-doped Co_3O_4 catalysts and their influence on the activities for NO and soot oxidation. Catal Sci Technol 7(20):4710–4719. https://doi.org/10.1039/c7cy01444a
12. Bin F, Song C, Lv G, Song J, Gong C, Huang Q (2011) $La_{1-X}K_xCoO_3$ and $LaCo_{1-Y}Fe_yO_3$ perovskite oxides: preparation, characterization, and catalytic performance in the simultaneous removal of NO_x and diesel soot. Ind Eng Chem Res 50(11):6660–6667. https://doi.org/10.1021/ie200196r
13. Rinkenburger A, Toriyama T, Yasuda K, Niessner R (2017) Catalytic effect of potassium compounds in soot oxidation. ChemCatChem 9(18):3513–3525. https://doi.org/10.1002/cctc.201700338
14. Mul G, Neeft JPA, Kapteijn F, Makkee M, Moulijn JA (1995) Soot oxidation catalyzed by a Cu/K/Mo/Cl catalyst: evaluation of the chemistry and performance of the catalyst. Appl Catal B Environ 6(4):339–352. https://doi.org/10.1016/0926-3373(95)00027-5
15. Marcilly C, Courty P, Delmon B (1970) Preparation of highly dispersed mixed oxides and oxide solid solutions by pyrolysis of amorphous organic precursors. J Am Ceram Soc 53(1):56–57. https://doi.org/10.1111/j.1151-2916.1970.tb12003.x
16. Shirley DA (1972) High-resolution x-ray photoemission spectrum of the valence bands of gold. Phys Rev B 5(12):4709–4714. https://doi.org/10.1103/PhysRevB.5.4709
17. Briggs D (1979). In: Wanger CD, Riggs WM, Davis LE, Moulder JF, Muilenberg GE (eds) Handbook of X-ray photoelectron spectroscopy. Perkin-Elmer Corp. Physical Electronics Division, Minnesota, pp 190–195
18. Umbach E (1992) Practical surface analysis. Wiley, New York
19. Dollimore D, Spooner P, Turner A (1976) The bet method of analysis of gas adsorption data and its relevance to the calculation of surface areas. Surf Technol 4(2):121–160. https://doi.org/10.1016/0376-4583(76)90024-8
20. Shannon RD (1976) Revised effective ionic radii and systematic studies of interatomic distances in halides and chalcogenides. Acta

Crystallogr Sect A 32(5):751–767. https://doi.org/10.1107/S0567739476001551
21. Naumkin VA, Kraut-Vass A, Gaarenstroom SW, J., P. C. (2012) NIST X-ray photoelectron spectroscopy database. Meas Serv Div Natl Inst Stand Technol. https://doi.org/10.18434/T4T88K
22. Galenda A, Natile MM, Krishnan V, Bertagnolli H, Glisenti A (2007) LaSrCoFeO and Fe_2O_3/LaSrCoFeO powders: synthesis and characterization. Chem Mater 19(11):2796–2808. https://doi.org/10.1021/cm062742i
23. Galenda A, Natile MM, Nodari L, Glisenti A (2010) $La_{0.8}Sr_{0.2}Ga_{0.8}Fe_{0.2}O_{3-\delta}$: influence of the preparation procedure on reactivity toward methanol and ethanol. Appl Catal B Environ 97(3–4):307–322. https://doi.org/10.1016/j.apcatb.2010.04.004
24. Lundin J, Engvall K, Holmlid L, Menon PG (1990) Mechanism of potassium loss by desorption from an iron oxide catalyst for the styrene process. Catal Lett 6(1):85–93. https://doi.org/10.1007/BF00764056
25. Lundin J, Hansson T, Pettersson JBC (1994) Kinetics for potassium desorption from an iron oxide catalyst studied by field reversal. Appl Surf Sci 74(4):343–349. https://doi.org/10.1016/0169-4332(94)90117-1
26. Joseph Y, Ketteler G, Kuhrs C, Ranke W, Weiss W, Schlögl R (2001) On the preparation and composition of potassium promoted iron oxide model catalyst films. Phys Chem Chem Phys 3(18):4141–4153. https://doi.org/10.1039/b104263g
27. Madey TE, Yakshinskiy BV, Ageev VN, Johnson RE (1998) Desorption of alkali atoms and ions from oxide surfaces: relevance to origins of Na and K in atmospheres of mercury and the moon. J Geophys Res E Planets 103(E3):5873–5887. https://doi.org/10.1029/98JE00230
28. Ura B, Trawczyński J, Kotarba A, Bieniasz W, Illán-Gómez MJ, Bueno-López A, López-Suárez FE (2011) Effect of potassium addition on catalytic activity of $SrTiO_3$ catalyst for diesel soot combustion. Appl Catal B Environ 101(3–4):169–175. https://doi.org/10.1016/j.apcatb.2010.09.018
29. Glisenti A, Pacella M, Guiotto M, Natile MM, Canu P (2016) Largely Cu-doped $LaCo_{1-X}Cu_xO_3$ perovskites for TWC: toward new PGM-free catalysts. Appl Catal B Environ 180:94–105. https://doi.org/10.1016/j.apcatb.2015.06.017
30. Onrubia JA, Pereda-Ayo B, De-La-Torre U, González-Velasco JR (2017) Key factors in Sr-doped $LaBO_3$ (B = Co or Mn) perovskites for NO oxidation in efficient diesel exhaust purification. Appl Catal B Environ 213:198–210. https://doi.org/10.1016/j.apcatb.2017.04.068
31. Ramesh K, Chen L, Chen F, Liu Y, Wang Z, Han YF (2008) Re-investigating the CO oxidation mechanism over unsupported MnO, Mn_2O_3 and MnO_2 catalysts. Catal Today 131(1–4):477–482. https://doi.org/10.1016/j.cattod.2007.10.061
32. Sihaib Z, Puleo F, Garcia-Vargas JM, Retailleau L, Descorme C, Liotta LF, Valverde JL, Gil S, Giroir-Fendler A (2017) Manganese oxide-based catalysts for toluene oxidation. Appl Catal B Environ 209:689–700. https://doi.org/10.1016/j.apcatb.2017.03.042
33. Sihaib Z, Puleo F, Pantaleo G, La Parola V, Valverde JL, Gil S, Liotta LF, Giroir-Fendler A (2019) The effect of citric acid concentration on the properties of $LaMnO_3$ as a catalyst for hydrocarbon oxidation. Catalysts 9(3):226. https://doi.org/10.3390/catal9030226
34. Neeft JPA, van Pruissen OP, Makkee M, Moulijn JA (1997) Catalysts for the oxidation of soot from diesel exhaust gases II. Contact between soot and catalyst under practical conditions. Appl Catal B Environ 12(1):21–31. https://doi.org/10.1016/S0926-3373(96)00060-4
35. Freund H-J (1997) Adsorption of gases on complex solid surfaces. Angew Chem Int Ed English 36(5):452–475. https://doi.org/10.1002/anie.199704521
36. Marsh H, Kuo K (1989) Kinetics and catalysis of carbon gasification. Introduction to carbon science. Butterworth-Heinemann, Oxford, pp 107–151
37. Prasad DH, Park SY, Oh EO, Ji H, Kim HR, Yoon KJ, Son JW, Lee JH (2012) Synthesis of nano-crystalline $La_{1-X}Sr_xCoO_{3-\delta}$ perovskite oxides by EDTA-citrate complexing process and its catalytic activity for soot oxidation. Appl Catal A Gen 447–448:100–106. https://doi.org/10.1016/j.apcata.2012.09.008
38. Li Z, Meng M, Zha Y, Dai F, Hu T, Xie Y, Zhang J (2012) Highly efficient multifunctional dually-substituted perovskite catalysts $La_{1-X}K_XCo_{1-Y}Cu_YO_{3-\delta}$ used for soot combustion, NO_x storage and simultaneous NO_x-soot removal. Appl Catal B Environ 121–122:65–74. https://doi.org/10.1016/j.apcatb.2012.03.022
39. Royer S, Duprez D, Kaliaguine S (2006) Oxygen mobility in $LaCoO_3$ perovskites. Catal Today 112(1–4):99–102. https://doi.org/10.1016/J.CATTOD.2005.11.020